Ionic Liquid Confined in MOF/Polymerized Ionic Network Host as a Solid Electrolyte for Lithium Batteries

Xiaolu Tian [a], *Yikun Yi* [a], *Zhendi Wu* [a], *Shentuo Zheng* [a], *Chao Shen* [b], *Binren Fang* [a], *Feng Hai* [a], *Jingyu Guo* [a], *Dmitry G. Shchukin*[c], *and Mingtao Li* [a,*]

[a]Shaanxi Key Laboratory of Energy Chemical Process Intensification School of Chemical Engineering and Technology, Xi'an Jiaotong University, No. 28, Xianning West Road, Xi'an, Shaanxi, 710049 (P. R. China).

[b]State Key Laboratory of Solidification Processing, Center for Nano Energy Materials, School of Materials Science and Engineering, Northwestern Polytechnical University and Shaanxi Joint Laboratory of Graphene (NPU), Xi'an, 710072 (P. R. China).

[c]Stephenson Institute for Renewable Energy, University of Liverpool, L69 7ZF, Liverpool (UK).
*E-mail: lmt01558@mail.xjtu.edu.cn (M.L.).

ABSTRACT

Ionic liquids (ILs) have been extensively studied as promising electrolytes for lithium batteries owing to their highly conductive and thermally stable characteristics. Although their

low t_{Li^+} and fluid nature can lead to weakened rate capability and higher leakage risks, these challenges can be tackled by incorporating ILs into solid hosts with controlled properties. Herein, we designed a heterogeneous metal organic framework (MOF)/polymerized ionic network (PIN) core-shell composite as a porous host for IL, DEME-TFSI. The PIN shell with abundant ionic structures not only exhibit nice compatibility with ILs to achieve high loading, but also provide transfer pathways through its charged backbone to fasten Li^+ transference; while the MOF core has narrow nanopores to confine large ions in ILs and enhance Li^+ selectivity. The as-synthesized conductive solid electrolyte (HKUST@PIN-IL-Li) showed intergrated merits of both MOF and PIN, including high IL loading, high ionic conductivity over 4×10^{-4} S cm^{-1} at 25 ^oC and increased Li^+ transfer number (0.367) in comparison to hollow H-PIN-IL-Li bare IL-Li electrolyte. The assembled $LiFePO_4$/Li solid batteries delivered a stable capacity of over 150 mAh g^{-1} for 100 cycles at 0.1 C and 130 mAh g^{-1} for 300 cycles at 0.5 C. Overall, our research demonstrates for the first time a novel MOF@PIN core-shell structure as a solid framework for IL with high performance.

TOC GRAPHICS

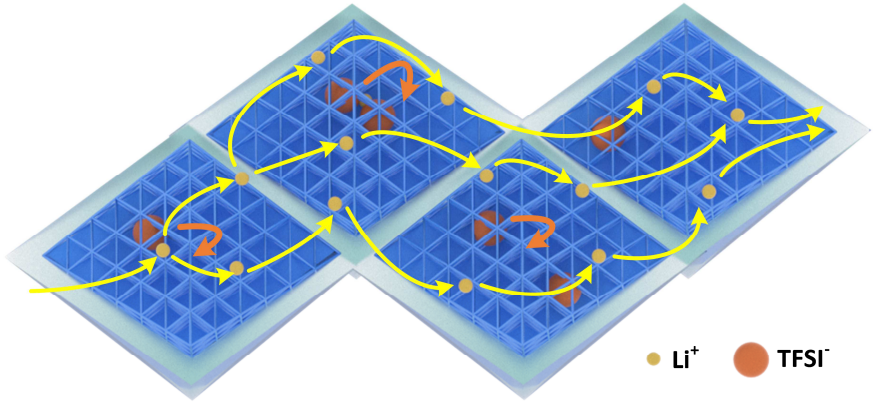

PIN shell connecting MOF particles for fast Li^+ transfer

Keywords: Polymerized Ionic Framework • Metal organic frameworks • Ionic liquid electrolytes • Solid electrolytes • Lithium batteries

1. Introduction

The high-power application of lithium ion battery (LIB) has been critically obstructed by its safety problems caused by traditional carbonate solvents.[1-2] Ionic liquids (ILs) are recognized as promising alternatives with negligible vapor pressure, non-flammability and electrochemical stability to solve the combustion and explosion risks of traditional LIBs.[3-7] However, the application of IL-based electrolyte is plagued by its low t_{Li^+}, fluid nature and poor separator infiltration.[8-11] To cope with this concern, ILs can be well impregnated into solid frameworks as solid-state composite electrolytes to prevent leakage risks while maintaining high ionic conductivity.[12-16] Besides, the frameworks with well-designed coordinate sites or fine channels

are capable of immobilizing the self-diffusion of large ions, thus realizing higher t_{Li^+}.

Common IL hosts include 1) porous carbon and silica materials; 2) zeolites; 3) traditional polymer matrices such as polyvinylidene fluoride (PVDF), polyether (PEO) and polymethyl methacrylate (PMMA); 4) ionic polymers such as poly(ionic liquid)s (PILs) and metal organic frameworks (MOFs).[14-15, 17-20] PILs with abundant ionic structures can provide transfer pathways for mobile ions through its charged backbone or pendant groups, and achieve high ionic conductivity (10^{-4}-10^{-3} S cm^{-1}).[21-22] The concentrated ionic structures can also realize favorable compatibility with IL ions to achieve high IL absorption (up to 200 wt% of PIL hosts).[20, 23-24] Polymerized ionic network (PIN) is one of the common PILs with repeating ionic units in its cross-linked backbone.[25-29] Zhao et al. found that the cross-linked network structures contributed to an ordered nature with more uniformly dispersed anion than linear PILs; Segalman et al. demonstrated that the ordered structure could promote ion mobility.[30-31] Tseng et al. reported a kind of PIL electrolyte cross linked by a dicationic imidazolium. The electrolyte exhibited high ionic conductivity (>10^{-4} S cm^{-1}) and stable battery performance at 25 ^{o}C and 60 ^{o}C.[32] But common PINs derived from nucleophilic substitution reactions between tertiary amine, phosphine, or imidazole and alkyl halide do not have proper two-dimensional structure and well-ordered nanopores, which limits their trap effects for mobile anions around the surface.[25]

On the contrary, metal organic frameworks (MOFs) with crystalline porous structures (5-20 Å), high specific surface area (1000-5000 m^2/g) and atomically precise skeletons are another emerging class of porous frameworks.[33-36] Their long-range order and well-defined nanopores

make them attractive hosts for IL electrolytes and provide fast Li^+ shuttling while reducing polymerization effects.[37] Incorporating ILs into MOFs pores to form remarkable MOF-IL composite electrolytes have been widely reported by previous researchers.[38-40] Fujie et al. found that [EMIM][TFSI] (1-ethyl-3-methylimidazolium bis(trifluoromethylsulfonyl)amide) IL showed restricted phase transition after incorporation into ZIF-8 host thus resulting in higher ionic conductivity at low temperature.[41] Li et al. designed a [EMIM][TFSI] in HKUST-1 solid electrolyte with high lithium transfer number of 0.46 at room temperature and good interfacial adhesion to cathode, but its low ionic conductivity (0.69×10^{-4} S cm^{-1}) led to limited cell capacity of only 80 mAh g^{-1} at 25 ^oC.[42] Wang et al. also reported a hot-activated HKUST-1 to load [EMIM][TFSI] electrolyte.[43] It was demonstrated that higher IL loading could enhance ionic conductivity and increase oxidation decomposition potential to 5.2 V. In the most reports of MOFs-IL composites, the loading amounts of IL electrolytes cannot usually exceed 100 wt% (of MOF hosts) based on the solid appearance, which is probably due to the less concentrated cationic density than PILs leading to weakened interactions and low conductivity.[44-48] To overcome these challenges, a heterogeneous MOF-in-PIN polymer framework can be designed for both high IL electrolytes absorption and enhanced selective transport of lithium-ions.

In this study, MOF@PIN core-shell particles were designed to realize high IL loading, ionic conductivity and selectivity of Li^+. On one hand, the MOF (HKUST-1) core with high surface area and aligned nanopores works as a mechanically and electrochemically stable framework to immobilize large mobile anions ($TFSI^-$) of IL and provide Li^+ conduction channels due to their

cationic unit. On the other hand, the PIN shell with high charge density serves as an IL-absorbing layer to prevent IL leakage from the MOF and provide a conductive pathway to transfer mobile ions along the ionic backbone. In addition, the PIN layer supported by MOF core exhibits better resistance to mechanical pressure than hollow PIN framework. Thus, by adding IL-LiTFSI filler into the MOF@PIN framework, a highly conductive composite electrolyte named as HKUST@PIN-IL-Li was synthesized. This electrolyte using heterogeneous HKUST@PIN framework has increased IL loading of 250 wt% and ionic conductivity of 4.07×10^{-4} S cm^{-1}, higher than the conductivity of MOF or PIN-only electrolyte. Besides, the t_{Li^+} of HKUST@PIN-IL-Li reaches 0.367, higher than that of PIN-only electrolyte (0.246) and pure IL electrolyte (0.176). The assembled $LiFePO_4$/Li solid batteries delivered a stable capacity of over 150 mAh g^{-1} for 100 cycles at 0.1 C, and 130 mAh g^{-1} for 300 cycles at 0.5 C, also higher and more stable than PIN-only electrolyte and pure IL electrolyte.

2. Experimental Section

Materials.

$Cu(NO_3)_2\cdot3H_2O$, 1,3,5-benzenetricarboxylic acid, 1,3,5-benzenetricarboxylic acid (BTC), 1,2,4,5-tetrakis(bromomethyl)benzene (TBB), 1,3,5-tri(1H-imidazol-1-yl)benzene (TIB), N,N-dimethylformamide (DMF), bistrifluoromethanesulfonimide lithium salt (LiTFSI) were purchased from Aladdin, China. All chemicals were used without further purification unless otherwise noted.

Synthesis of DEME-TFSI ionic liquid.

In the typical synthesis, diethylmethylamine (0.1 mol) and 1-bromo-2-methoxyethane (0.1 mol) were dissolved in 10 ml acetonitrile. The solution was heated at 40 °C for 12 h under N_2 atmosphere. The resulting pale yellow solution was then washed with ethanol to obtain DEME-Br white solid, which was dried at 60 °C overnight. The DEME-Br was dissolved in LiTFSI aqueous solution for ion exchange. Dichloromethane was then added to extract DEME-TFSI, which was washed 3 times with water. The resulting DEME-TFSI ionic liquid was dried in vacuum at 100 °C overnight to remove water.

Synthesis of HKUST-1.

In a typical synthesis, 1.22 g (5.24 mmol) $Cu(NO_3)_2 \cdot 3H_2O$ and 0.58 g (2.76 mmol) BTC were dissolved in 5 g dimethyl sulfoxide (DMSO) to form a homogeneous precursor solution. 500 uL precursor solution was dropped into 10 mL methanol during 1 min with continuous stirring. Then, the blue suspension was kept stirring for 10 min and washed 3 times by methanol to get HKUST-1 product. The HKUST-1 was further dried at 60 °C under vacuum to remove excess of solvent.

Synthesis of PIN.

56 mg (0.125 mmol) TBB and 46 mg TIB were dispersed in a mixture containing 40 mL acetonitrile and 10 mL DMF. After ultrasonic treatment, the suspension was transferred to 85 °C oil bath and kept for 5 h. The obtained white product (PIN-Br) was collected by centrifugation

and washed three times with acetonitrile, followed by drying at 60 °C under vacuum for 8 h. The PIN-Br was then dispersed and stirred in a LiTFSI aqueous solution at a mole ratio of Br^-: $TFSI^-$ = 1 : 1.5 at 60 °C overnight for ion exchange. The solid product was obtained by filtration and washed with deionized water. The final product was dried at 100 °C in vacuum overnight to remove water and obtain PIN.

Synthesis of HKUST-1@PIN.

100 mg HKUSTI-1 and 56 mg (0.125 mmol) TBB were dispersed in a mixture of 20 mL acetonitrile and 5 mL DMF. 1. 46 mg TIB was dispersed in a mixture containing 20 mL acetonitrile and 5 mL DMF. After ultrasonic treatment, these two suspensions were mixed and transferred to 85 °C oil bath and kept for 5 h. The obtained glaucous product (HKUSTI-1@PIN-Br) was collected by centrifugation and washed three times with acetonitrile followed by drying at 60 °C under vacuum for 8 h. The HKUSTI-1@PIN-Br was then dispersed and stirred in LiTFSI aqueous solution at a mole ratio of Br^- : $TFSI^-$ = 1 : 1.5 at 60 °C overnight for ion exchange. The solid product was obtained by filtration and washed with deionized water. The final product was dried at 100 °C in vacuum overnight to remove water and obtain HKUSTI-1@PIN.

Synthesis of hollow PIN (H-PIN).

The as-synthesized HKUST-1@PIN was washed by excess HCl and deionized water to remove HKUST-1 core. The white product was dried at 80 °C under vacuum overnight to obtain

H-PIN.

Characterization.

X-ray diffraction (XRD) measurements were carried out on a Riguku D/MAX2550 diffractometer with Cu-Kα radiation operating at a voltage of 50 kV and a current of 200 mA.

X-ray photoelectron spectroscopy (XPS, ESCALAB Xi+, Thermo Scientific) was performed by using a monochromatized Al Kα (1486.6 eV) X-ray source. The data processing (peak fitting) was performed with the XPSPEAK41 software using a Shirley type background subtraction and Gaussian/Lorentzian peak shapes. The binding energies were corrected by setting the C1s hydrocarbon (–CH2–CH2– bonds) peak at 284.6 eV.

The surface morphology of lithium anodes was characterized by scanning electron microscopy (SEM) (GeminiSEM 500). The instrument uses an electron beam accelerated at 10 kV enabling operation at a variety of currents. The Li anode samples were obtained by disassembling coin cells after 200 charge-discharge cycles. The separated Li anode was further washed by DME to remove electrolyte residuals on its surface. To avoid air contamination, the Li electrode samples were transferred in the sealed box filled with argon gas and loaded into the SEM machine under argon atmosphere.

Electrochemical measurements.

The ionic conductivity of the COFs-DEME electrolytes was determined from the

impedance spectrum using a blocking cell of which the electrolyte was sandwiched between two stainless steel electrodes in a Swagelok cell using a hydropress under 2 MPa. Electrochemical impedance spectrum measurements were performed using a CHI760 electrochemical workstation over a frequency range of 0.1 Hz to 100 kHz with a potential static signal amplitude of 10 mV. Linear sweep voltammetry was performed at 25 ^{o}C (scan rate 10 mV s^{-1}) using a stainless steel/electrolyte/Li Swagelok cell.

Battery test.

Lithium foil (battery grade) was used as a negative electrode. The positive electrode was fabricated by spreading the mixture of LiFePO4, Super P, and PVDF (initially dissolved in N-methyl-2-pyrrolidone) with a weight ratio of 8:1:1 onto an aluminum current collector (battery use). Li/$LiFePO_4$ batteries were fabricated (in an argon-filled glove box) by laminating the Li foil, the electrolyte and a $LiFePO_4$ cathode tape in a coin cell.

Preliminary cycling tests on Li/$LiFePO_4$ batteries were performed at 25 ^{o}C using a CT2001A cell test instrument (Neware Electronic Co., Ltd.). The charge and discharge current rates were fixed to 0.1 C, 0.5 C and 1 C. The voltage cutoffs were fixed at 4.0 V (charge step) and 2.0 V (discharge step), respectively.

3. Results and discussion

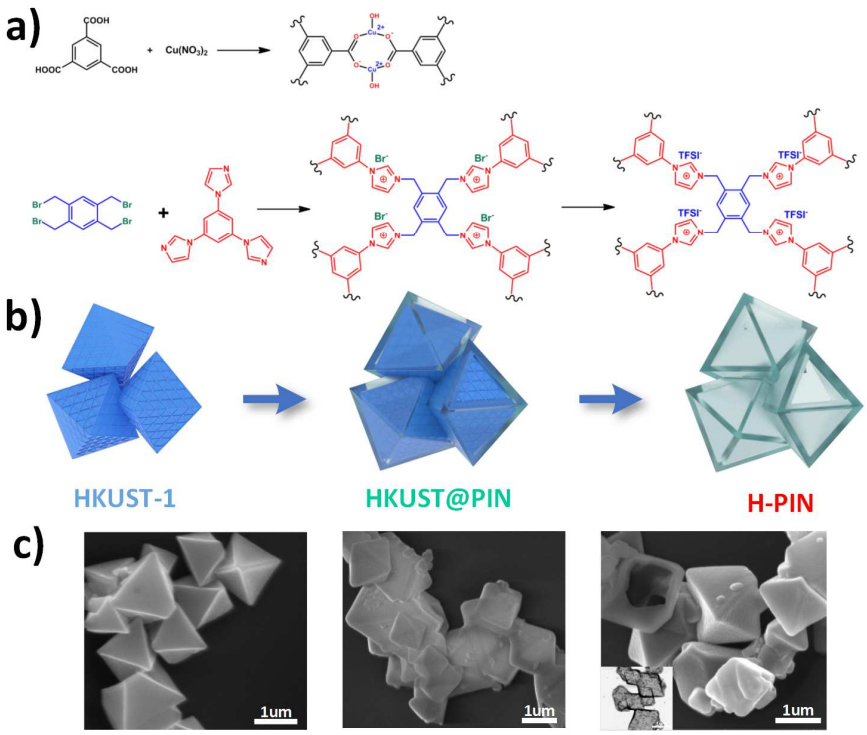

Figure 1. a) The synthetic procedure to obtain HKUST-1 and PIN. b) A schematic diagram of fabricating HKUST@PIN and H-PIN. c) SEM images of HKUST-1, HKUST@PIN and H-PIN samples, respectively. Inset shows the TEM image of H-PIN sample.

The synthesis of core-shell HKUST@PIN particles is illustrated in Figure 1. Briefly, HKUST-1 was firstly prepared using $Cu(NO_3)_2$ and BTC as the core template. The resulting HKUST-1 particles were then mixed with TIB and TBB to form in-situ PIN shell outside the particle.

According to the SEM images, the size of the HKUST-1 particle is around 1 um, and the HKUST@PIN shows a similar size of 1um. Different from the nanoparticle morphology of the template-free PIN sample (Figure 1), the PIN layer is uniformly deposited on the surface of

HKUST-1 particles. As a comparison, the HKUST-1 core was removed to get (H-PIN) as another framework, where the hollow space is expected to accommodate more IL electrolyte. The hollow structure can be demonstrated by the several cracked particles in the SEM images of H-PIN sample (Figure 1c). The TEM images of H-PIN further confirm that hollow PIN frameworks are left after the removal of HKUST-1 core.

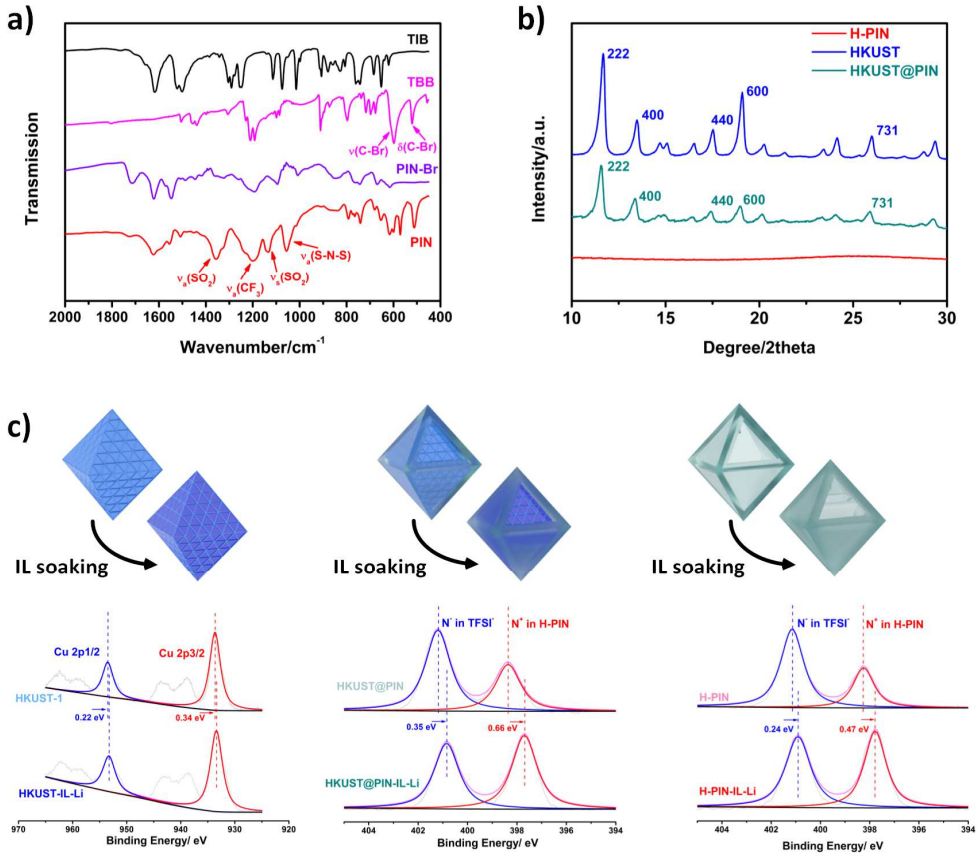

Figure 2. a) Fourier Transform Infrared spectra of reactant TIB, TBB and product PIN-Br, PIN. b) X-ray diffraction patterns of HKUST-1, HKUST@PIN and H-PIN. c) Cu2p XPS curves of HKUST-1 and HKUST-IL-Li; N1s XPS curves of HKUST@PIN and HKUST@PIN-IL-Li; N1s XPS curves of H-PIN and H-PIN-IL-Li, respectively.

The Fourier-transform infrared (FTIR) spectra of TIB, TBB, synthesized PIN-Br and PIN are shown in Figure 2a. By comparing the FTIR curves of TBB and PIN-Br, the disappearance of ν(C-Br) (598 cm^{-1}) and δ(C-Br) (521 cm^{-1}) peaks indicates that PIN-Br is successfully synthesized through a nucleophilic substitution reaction. In the FTIR curve of PIN, four peaks appear at 1060, 1135, 1188, 1344 cm^{-1} attributed to the ν_a(S-N-S), $\nu_s(SO_2)$, $\nu_a(CF_3)$, and $\nu_a(SO_2)$ of $TFSI^-$ anions, respectively, suggesting the ion exchange from Br^- to $TFSI^-$ in the PIN framwork. The XRD patterns (Figure 2b) show the crystallinity of HKUST-1 particle and the crystalline structure is well retained after PIN coating according to the pattern of HKUST@PIN. By contrast, no characteristic diffraction peak can be observed from the XRD pattern of H-PIN indicating the complete removal of HKUST-1 core.

To fabricate polymer-IL composite electrolyte, certain amounts of [DEME][TFSI]-LiTFSI (IL-Li) electrolyte are incorporated into HKUST-1, PIN, HKUST@PIN and H-PIN through mechanical mixing, respectively. All of the hosts are mixed with as much IL-Li as possible based on the solid appearance, and the resulting IL loadings are 80%, 130%, 250%, and 280% (mass ratio) of HKUST-1, PIN, HKUST@PIN, and H-PIN, respectively. It is reasonable that the HKUST@PIN and H-PIN can load more IL than solid PIN particles because extra IL electrolytes are trapped in the HKUST-1 core framework. The H-PIN shows the highest IL loading because the HKUST-1 core framework is cleared as hollow space.

The Cu 2p XPS was conducted to investigate the ionic interaction between Cu cationic centers in HKUST-1 and $TFSI^-$ in IL. As is shown in Figure 2c, the pristine HKUST-1 exhibits

binding energies of Cu 2p at 954.87 and 934.95 eV, respectively. For the HKUSTI-IL-Li composite electrolyte, the binding energies are negatively increased by 0.22 and 0.34 eV, because the electron cloud density of Cu centers are increased when they form interactions with $TFSI^-$ anions. The ionic interactions between quaternary ammonium cations in PIN shell and $TFSI^-$ in IL are investigated in the same way using N1s spectroscopy in Figure 2c. The N1s peaks of the HKUST@PIN samples show two peaks at 401.20 eV and 398.36 eV, which are attributed to the pyridinum N^+ in cationic PIN and N^- in TFSI anions, respectively. After the introduction of IL electrolytes, the N^+ peak of HKUST@PIN-IL-Li also exhibits negative shift by 0.66 eV suggesting the negative charge of N^+ backbone when interacting with the added TFSI anions. Similarly, H-PIN samples exhibit negative peak shift by 0.47 eV, which is lower than that in HKUST@PIN XPS spectrum. The lower peak shift of H-PIN indicates weakened interactions between PIN layer and IL anions, probably because the hollow structure of H-PIN is damaged by mechanical pressure during XPS sample preparation leading to the leakage of dissociative IL. In conclusion, the PIN coated HKUST-1 particles (HKUST@PIN) exhibit better compatibility with IL-Li than bare HKUST-1 particles in terms of IL loading and ionic interactions. Although H-PIN can load the most IL into its hollow space, it turns out to be an undesirable candidate as solid framework because the removal of MOF core leads to structural instability and IL loss.

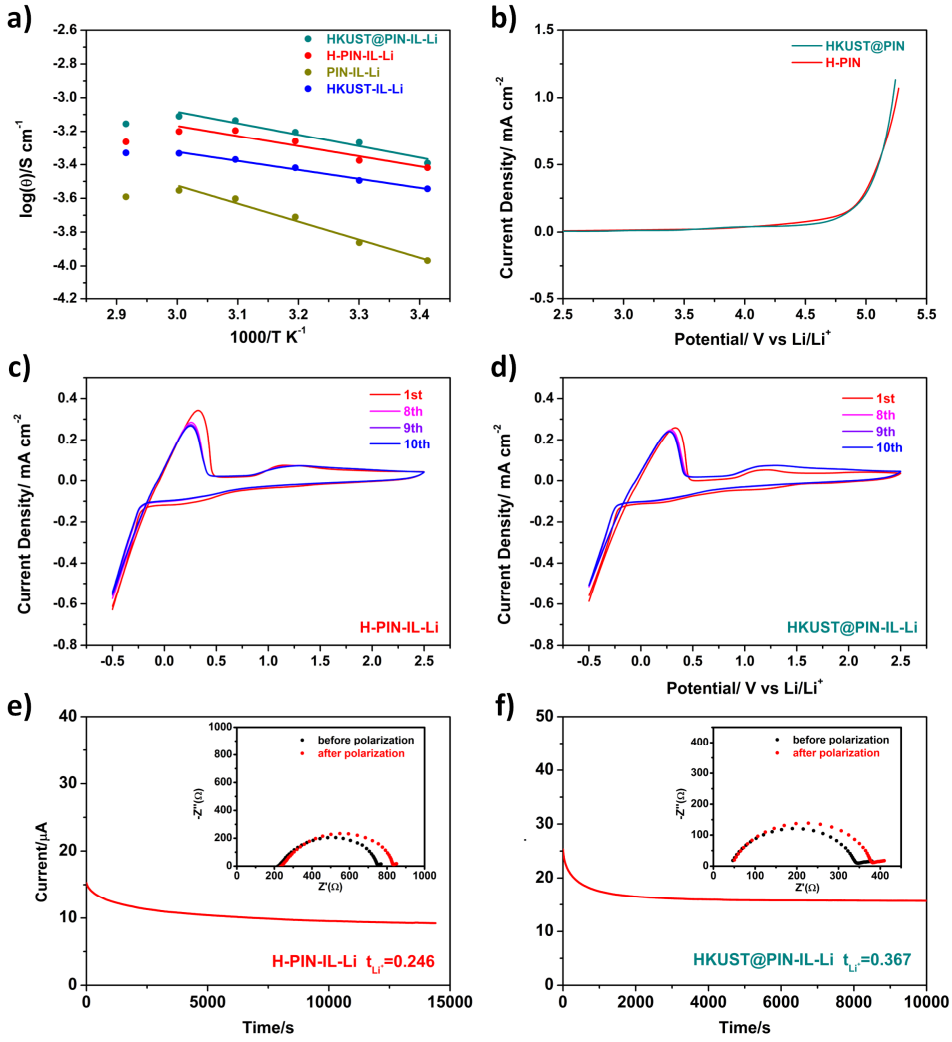

Figure 3. a) Temperature dependence of the ionic conductivity of HKUST-IL-Li, PIN-IL-Li, HKUST@PIN-IL-Li and H-PIN-IL-Li electrolytes. b) LSV curves at a scan rate of 10 mV s^{-1} for HKUST@PIN-IL-Li and H-PIN-IL-Li composite electrolytes (SS//Li cells). c,d) CV curves for H-PIN-IL-Li and HKUST@PIN-IL-Li electrolytes, respectively. Working electrode: stainless steel; counter electrode and reference electrode: lithium; scan rate: 10 mV s^{-1}. e,f) Chronoamperometry responses of H-PIN-IL-Li and HKUST@PIN-IL-Li electrolytes to the

applied potential of 10 mV; inset shows the cell impedance response (Nyquist plot) before and after polarization.

The ionic conductivity as a function of temperature for HKUST-IL-Li, PIN-IL-Li, H-PIN-IL-Li and HKUST@PIN-IL-Li electrolytes was evaluated by AC impedance techniques at room temperature. The results are presented in Figure 3a. It can be observed that from 20 ^{o}C ~ 60 ^{o}C, the ionic conductivity of all electrolytes linearly increases with increasing temperature for motivated migration of carrier ions, roughly following the Arrhenius rule. As the temperature rises to 70 ^{o}C, the conductivity begins to decrease. This is reasonable because at high IL loading, the transportation of mobile ions is found to be blocked because of collective field-induced interactions, which suppress the ionic mobility and tremendously decrease the conductivity.[49] The coated HKUST@PIN-IL-Li and hollow H-PIN-IL-Li were calculated to show higher ionic conductivity than bare HKUST-IL-Li and solid PIN-IL-Li electrolytes due to their much higher IL loading. The H-PIN loading 280% IL-Li is less conductive (3.82 $\times 10^{-4}$ S cm^{-1} at 20 ^{o}C) than HKUST@PIN loading 250% IL-Li (4.07 $\times 10^{-4}$ S cm^{-1} at 20 ^{o}C) mainly for its mechanical instability as mentioned above. In conclusion, both of the electrolytes are conductive enough for practical application in room-temperature lithium batteries.

The electrochemical stability of H-PIN-IL-Li and HKUST@PIN-IL-Li electrolytes are characterized by linear sweep voltammetry (LSV) using Li//SS cells in Figure 3b. Both of the electrolytes showed no decomposition current until around 5.0 V vs Li/Li^{+}, higher than the working voltage range of lithium batteries. Lithium redox performance in the

HKUST@PIN-IL-Li and H-PIN-IL-Li electrolytes is also determined by cyclic voltammograms (CVs) test with Li//SS cells. It can be clearly observed from Figures 3c and 3d that the plating and stripping of lithium occur on the SS electrode. In the first cycle of H-PIN-IL-Li, the Li plating peak at -0.23 V versus Li/Li^+ and the Li stripping peak at 0.32 V versus Li/Li^+ suggest successful Li redox in the H-PIN-IL-Li electrolytes. The CV current gradually decreases to a steady state until the 8-10th cycles which can be assigned to the formation of a stable solid electrolyte interface (SEI) on the SS electrode. In addition to the Li redox peaks, the anodic peak at 1.13 V versus Li/Li^+ is due to the formation of Li-SS alloys. The HKUST@PIN-IL-Li electrolyte also exhibits a similar CV curve with Li redox peaks at -0.23 V and 0.32 V versus Li/Li^+. According to the peak current value, the CV curve of HKUST@PIN-IL-Li is more stable with the increase number of cycles for its better particle stability supported by HKUST-1 template than H-PIN-IL-Li.

To verify the Li^+ selectivity of HKUST@PIN and H-PIN frameworks, the t_{Li}^+ of HKUST@PIN-IL-Li, H-PIN-IL-Li, and IL-Li is characterized by DC polarization in Li/electrolyte/Li cells with an applied potential of 10 mV. As is shown in Figure 4e and 4f, the calculated t_{Li}^+ of bare IL-Li is only 0.176 according to Equation (1), due to the free transfer of large cations and anions of IL. The t_{Li}^+ of H-PIN-IL-Li is 0.246 (Figure 4e), slightly improved than IL-Li because of the immobilization of $TFSI^-$ by cationic PIN. From Figure 4f, the HKUST@PIN-IL-Li shows a higher t_{Li}^+ of 0.367, which can be attributed to the more remarkable confinement of $TFSI^-$ in the ordered nanopores of HUKST-1 core. The HKUST-1

framework confines mobile anions for not only its narrow pore size close to $TFSI^-$ but also the electrostatic force of positive Cu centers, while for H-PIN framework most ILs are in unbound state in the hollow space. The HKUST@PIN-IL-Li significantly enhances the transfer efficiency by 209%, and achieves a high Li^+ conductivity up to 1.49×10^{-4} S cm^{-1}.

$$t_{Li^+} = \frac{I_{SS}(\Delta V - I_0 R_0)}{I_0(\Delta V - I_{SS} R_{SS})} \quad (1)$$

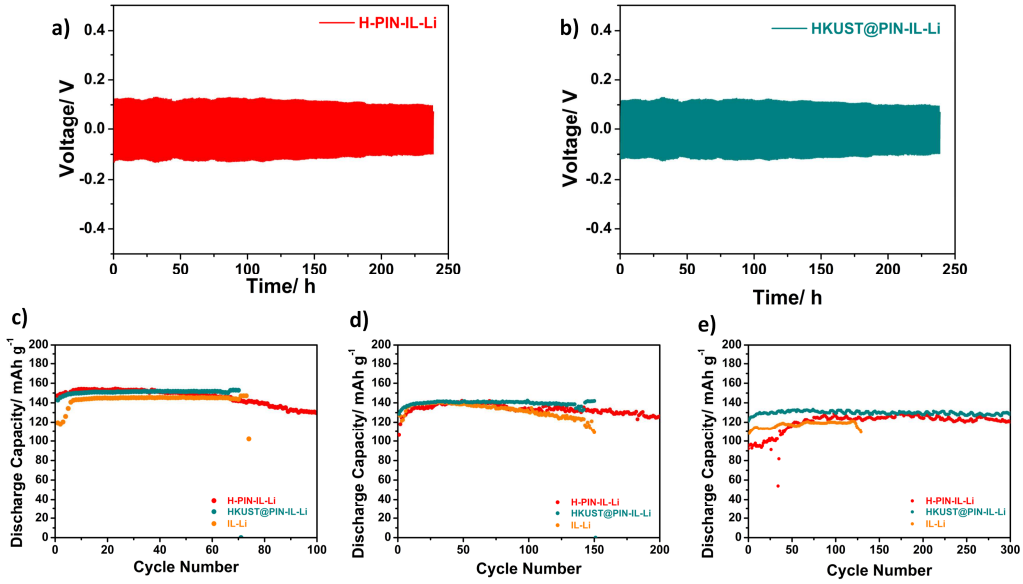

Figure 4. a,b) Voltage profiles of the lithium plating/striping cycling for HKUST@PIN-IL-Li and H-PIN-IL-Li electrolytes at a current density of 0.1 mA cm^{-2} at room temperature, respectively. Discharge capacity as a function of cycle number for bare IL-Li, HKUST@PIN-IL-Li and H-PIN-IL-Li electrolytes in Li//$LiFePO_4$ and cells at room temperature at c) 0.1 C, d) 0.2 C and c) 0.5 C.

To investigate the interfacial stability of HKUST@PIN-IL-Li and H-PIN-IL-Li composite

electrolytes against Li metal anode, the Li stripping/plating experiments were conducted in Li//Li cells (Figure 4a,b). The cells are kept at room temperature and charged under a current density of 0.1 mA cm^{-2} for 1 h in each cycle. Both of the HKUST@PIN-IL-Li and H-PIN-IL-Li electrolytes exhibit an initial overpotential of 116 mV and 130 mV and keep smooth at 95.8 and 98.0 mV, respectively, for over 300 h without violent vibration suggesting the stable lithium stripping/plating performance and interfacial compatibility.

$LiFePO_4$//Li cells were fabricated and tested at 0.1 C to investigate the practical application of PIN-based electrolytes in solid lithium batteries (Figure 4c). The $LiFePO_4$/IL-Li/Li cell demonstrated a discharge capacity increase to over 150 mAh g^{-1}.

4. Conclusions

In this work, we designed a heterogeneous MOF/PIN core-shell framework to host IL (DEME-TFSI) as a solid-state electrolytes for lithium batteries. The fabricated solid electrolyte (HKUST@PIN-IL-Li) inherits the merits of both MOF and PIN exhibiting high IL loading (IL : MOF@PIN = 1 :2.8 wt%), high ionic conductivity over 4×10^{-4} S cm^{-1} at 25 ^{o}C and increased Li^{+} transfer number (0.367) in comparison to hollow H-PIN-IL-Li (0.246) bare IL-Li electrolyte (0.176), suggesting a synergistic effect of MOF/PIN on Li^{+} transference efficiency due to their confinement of $TFSI^{-}$ anions in IL. The assembled $LiFePO_4$/Li solid batteries with HKUST@PIN-IL-Li electrolytes deliver a stable capacity of over 150 mAh g^{-1} for 100 cycles at 0.1 C, and 130 mAh g^{-1} for 300 cycles at 0.5 C. Overall, our work provides a rational design of

MOF/PIN core-shell structure to host IL and achieve effecient Li^+ transfer, which can be extended to other core-shell materials for the tunability of MOFs and PILs.

ASSOCIATED CONTENT

Supporting Information.

The Supporting Information is available free of charge at DOI:

AUTHOR INFORMATION

Corresponding author

*E-mail: lmt01558@mail.xjtu.edu.cn (M.L.).

Declaration of competing interest

The authors declare no competing financial interest.

Acknowledgements

Financial support from the Natural Science Foundation of China (grant no. 21978231, 21773223) and Jiangsu Provincial Department of Science and Technology (BK20201190). We thank the Instrumental Analysis Center of Xi'an Jiaotong University for material characterizations.

References

[1] S. Y. Chen, Z. H. Gao, T. J. Sun, Energy Sci. Eng. 2021, 9, 1647-1672.

[2] D. H. Liu, Z. Y. Bai, M. Li, A. P. Yu, D. Luo, W. W. Liu, L. Yang, J. Lu, K. Amine, Z. W. Chen, Chem. Soc. Rev. 2020, 49, 5407-5445.

[3] C. F. J. Francis, I. L. Kyratzis, A. S. Best, Advanced Materials 2020, 32.

[4] E. Kim, J. Han, S. Ryu, Y. Choi, J. Yoo, Materials 2021, 14.

[5] K. Liu, Z. Wang, L. Shi, S. Jungsuttiwong, S. Yuan, Journal Of Energy Chemistry 2021, 59, 320-333.

[6] L. M. McGrath, J. F. Rohan, Molecules 2020, 25.

[7] W. Zhou, M. Zhang, X. Kong, W. Huang, Q. Zhang, Advanced Science 2021, 8.

[8] C. Liao, N. Shao, K. S. Han, X.-G. Sun, D.-E. Jiang, E. W. Hagaman, S. Dai, Physical Chemistry Chemical Physics 2011, 13, 21503-21510.

[9] P. Yang, X. Gao, X. Tian, C. Shu, Y. Yi, P. Liu, T. Wang, L. Qu, B. Tian, M. Li, W. Tang, B. Yang, J. B. Goodenough, Acs Energy Letters 2020, 5, 1681-1688.

[10]Z. Wang, Z. Wang, L. Yang, H. Wang, Y. Song, L. Han, K. Yang, J. Hu, H. Chen, F. Pan, Nano Energy 2018, 49, 580-587.

[11] A. Lewandowski, A. Swiderska-Mocek, Journal Of Power Sources 2009, 194, 601-609.

[12] D. M. Correia, L. C. Fernandes, P. M. Martins, C. Garcia-Astrain, C. M. Costa, J. Reguera, S. Lanceros-Mendez, Advanced Functional Materials 2020, 30.

[13] J. Hwang, K. Matsumoto, C.-Y. Chen, R. Hagiwara, Energy & Environmental Science 2021.

[14] A. A. Shamsuri, R. Daik, S. N. A. M. Jamil, Processes 2021, 9.

[15] G. Yang, Y. Song, Q. Wang, L. Zhang, L. Deng, Materials & Design 2020, 190.

[16] S.-Y. Zhang, Q. Zhuang, M. Zhang, H. Wang, Z. Gao, J.-K. Sun, J. Yuan, Chem. Soc. Rev. 2020, 49, 1726-1755.

[17] Y. Li, Z. Sun, L. Shi, S. Lu, Z. Sun, Y. Shi, H. Wu, Y. Zhang, S. Ding, Chemical Engineering Journal 2019, 375.

[18] B. Niu, S. Luo, C. Lu, W. Yi, J. Liang, S. Guo, D. Wang, F. Zeng, S. Duan, Y. Liu, L. Zhang, B. Xu, Solid State Ionics 2021, 361.

[19] X. Tian, P. Yang, Y. Yi, P. Liu, T. Wang, C. Shu, L. Qu, W. Tang, Y. Zhang, M. Li, B. Yang, Journal Of Power Sources 2020, 450.

[20] Z. Wang, W. Zheng, W. Sun, L. Zhao, W. Yuan, Acs Applied Energy Materials 2021, 4, 2808-2819.

[21] X. Wang, W. Hong, Applied Physics Letters 2011, 98.

[22] M. Watanabe, H. Tokuda, S. Muto, Electrochim. Acta 2001, 46, 1487-1491.

[23] S. A. Alexandre, G. G. Silva, R. Santamaria, J. P. C. Trigueiro, R. L. Lavall, Electrochim. Acta 2019, 299, 789-799.

[24] M. Brinkkotter, E. I. Lozinskaya, D. O. Ponkratov, Y. Vygodskii, D. F. Schmidt, A. S. Shaplov, M. Schonhoff, J. Phys. Chem. C 2019, 123, 13225-13235.

[25] P. Zhang, M. Li, B. Yang, Y. Fang, X. Jiang, G. M. Veith, X.-G. Sun, S. Dai, Advanced Materials 2015, 27, 8088-8094.

[26] X. L. Tian, Y. K. Yi, P. Yang, P. Liu, L. Qu, M. T. Li, Y. S. Hu, B. L. Yang, Acs Applied Materials & Interfaces 2019, 11, 4001-4010.

[27] X. Li, Y. Zheng, Q. Pan, C. Y. Li, Acs Applied Materials & Interfaces 2019, 11, 34904-34912.

[28] K. Matsumoto, S. Sogabe, T. Endo, Journal Of Polymer Science Part a-Polymer Chemistry 2012, 50, 1317-1324.

[29] C. Shen, Q. Zhao, C. M. Evans, Advanced Materials Technologies 2019, 4.

[30] C. M. Evans, C. R. Bridges, G. E. Sanoja, J. Bartels, R. A. Segalman, ACS Macro Lett. 2016, 5, 925-930.

[31] Q. J. Zhao, C. T. Shen, K. P. Halloran, C. M. Evans, ACS Macro Lett. 2019, 8, 658-663.

[32] Y. C. Tseng, F. I. Ramdhani, S. H. Hsiang, T. Y. Lee, H. S. Teng, J. S. Jan, J. Membr. Sci. 2022, 641, 11.

[33] Q. Wang, D. Astruc, Chemical Reviews 2020, 120, 1438-1511.

[34] Z. Wang, S. Wang, A. Wang, X. Liu, J. Chen, Q. Zeng, L. Zhang, W. Liu, L. Zhang, Journal Of Materials Chemistry A 2018, 6, 17227-17234.

[35] A. Bavykina, N. Kolobov, I. S. Khan, J. A. Bau, A. Ramirez, J. Gascon, Chemical Reviews 2020, 120, 8468-8535.

[36] H. Zhong, Y. Wang, C. Cui, F. Zhou, S. Hu, R. Wang, Chem. Sci. 2018, 9, 8703-8710.

[37] X. Tian, S. Chen, P. Zhang, P. Yang, Y. Yi, T. Wang, B. Fang, P. Liu, L. Qu, M. Li, H. Ma, Electrochim. Acta 2021, 389.

[38] A. Singh, R. Vedarajan, N. Matsumi, Journal Of the Electrochemical Society 2017, 164, H5169-H5174.

[39] Q. Xu, X. Zhang, S. Zeng, L. Bai, S. Zhang, Acs Sustainable Chemistry & Engineering 2019, 7, 7892-7899.

[40] X. Yu, N. S. Grundish, J. B. Goodenough, A. Manthiram, Acs Applied Materials & Interfaces 2021, 13, 24662-24669.

[41] K. Fujie, K. Otsubo, R. Ikeda, T. Yamada, H. Kitagawa, Chem. Sci. 2015, 6, 4306-4310.

[42] M. Li, T. Chen, S. Song, Y. Li, J. Bae, Nanomaterials 2021, 11, 13.

[43] Z. T. Wang, H. Zhou, C. F. Meng, W. W. Xiong, Y. J. Cai, P. F. Hu, H. Pang, A. H. Yuan, Acs Applied Energy Materials 2020, 3, 4265-4274.

[44] R. Dutta, A. Kumar, Journal Of Materials Science-Materials In Electronics 2019, 30, 1117-1132.

[45] R. Dutta, A. Kumar, in 24th Condensed Matter Days National Conference (CMDAYS), Vol. 765, Mizoram Univ, Phys Dept, Aizwal, INDIA, 2016.

[46] V. Nozari, C. Calahoo, J. M. Tuffnell, P. Adelhelm, K. Wondraczek, S. E. Dutton, T. D. Bennett, L. Wondraczek, Scientific Reports 2020, 10.

[47] Q. Xu, F. Yang, X. Zhang, J.-R. Li, J.-F. Chen, S. Zhang, Chemelectrochem 2020, 7, 183-190.

[48] Y. Yoshida, H. Kitagawa, Acs Sustainable Chemistry & Engineering 2019, 7, 70-81.

[49] A. B. Kanj, R. Verma, M. D. Liu, J. Helfferich, W. Wenzel, L. Heinke, Nano Lett. 2019, 19, 2114-2120.